Technological characterization of PE/EVA blends for foam injection molding

Technological characterization of PE/EVA blends for foam injection moulding

Roberto SPINA [1,a*]

[1] Dept. of Mechanics, Mathematics and Management (DMMM), Politecnico di Bari, Bari (Italy)
[a] roberto.spina@poliba.it

Abstract. The foam injection moulding is one of the most important processes to produce lightweight plastic parts. The main feature of this process is the use of a foam blowing agent (physical or chemical) that decomposes during heating, generating gasses that are dispersed into the melt. Predicting the final part microstructure requires the investigation of the foam process which is a complex problem because it is necessary to combine transport phenomena of the multi-phase flow in non-isothermal conditions with foam kinetics and gas formation. The aim of this work is to evaluate the material-processing relationship in foam injection moulding. The experimental measurements of PE/EVA blends, properly formulated, coupled to two types of ADC foaming agents are carried-out with differential scanning calorimetry and rotational rheometry. The injection moulding and direct measurements of foamed parts are then performed, based on previous measurements, to evaluate the process performances.

Keywords: Foam Injection moulding, Material characterization, Differential scanning calorimetry, Rotational rheometry.

1. Introduction

Polymer foaming represents one of the main strategic techniques for the production of low density, highly thermal and acoustic insulating, shock adsorbing materials. Thermoplastic polymer foams can be obtained by extrusion, injection moulding and rotational moulding, as reported by *Hornsby* [1]. The foam injection moulding is very interesting for realizing very complex shaped parts. The research effort is actually focused on improving knowledge of material properties and enhancing product and process performances, as *Liu et al.* [2] point out.

The blowing agent plays a critical role in manufacturing the foam part as well as in mould and product design. *Allen et al.* [3] investigated the expansion process of ethylene-vinyl acetate (EVA) to automatically compute the mould cavity geometry from the final part geometry. The used approach considers the foam injection moulding of several basic shapes (primitives), the analysis of the expansion characteristics and their combination into the final shape of the manufactured part. *Barzegari et al.* [4] studied the flexural modulus of symmetric structural high density polyethylene (HDPE) and low density polyethylene (LDPE) foams with complex density distribution across thickness. The results indicate that the average cell size and cell size distribution of HDPE foams are smaller than LDPE foams.

From a material processing point of view, several studies were done to evaluate the influence of blowing agents on main material properties as well as variations in material properties. *Solorzano and Rodriguez-Perez* [5] point out that the choice of a blowing agent and the final processing conditions are linked. In the case of foaming of thermoplastics, the blowing agent may modify the melt viscosity and/or the temperature of the polymer and thus the melt rheological properties during foam formation. *Reyes-Labarta and Marcilla* [6] investigated the different transitions and reactions involved in the thermal processing of EVA-PE-ADC mixtures with different concentrations of polyethylene (PE) and azodicarbonamide (ADC). They used Differential Scanning Calorimetry (DSC) analysis which allows a better knowledge of the phenomena involved during foaming in order to control and optimize the processing conditions. *Zhang et al.* [7] studied the crystallization, rheological, and mechanical behaviuor of HDPE/EVA blends with selective cross-linking in the EVA phase. The rheological measurements and microscopic observations reveal that the non-cross-

linked blends show a better stability compared to the cross-linked blends. *Vachon* [8] investigated alternative blowing agents in foam injection moulding. His research points out that the agents should be combined with other additives (activators, cross-linking agents, etc.) to achieve the optimal processing conditions. In addition the polymer rheology must be accurately controlled because its viscosity and resistance to deformation will determine the lowest reachable foam density. *Greco et al.* [9] studied the foaming process of recycled polymers to increase the diversification of recycling and explore potential markets. The authors evaluate the applicability of different grades of recycled PE foamed with a recycled gypsum, performing analyses with DSC and a capillary rheometry. The results point out that the foamed parts have a lower density compared to those foamed with ADC. *Antunes and Velasco* [10] studied the development of novel lightweight polymer nano-composites by combining foaming with the addition of small amounts of nano-sized fillers to create multifunctional polymer foams that overcome the high cost of the conductive polymers. The authors focus their research on the use of conductive carbon-based nanoparticles in emerging sectors such as aerospace or leading sectors such as electronics. The process itself was also investigated to improve its performance. *Li et al.* [11] investigated the mechanical behaviuor of foam under complex loading conditions in service over different spectrums of strain. The authors use a continuous indentation test and inverse finite element modelling to determine the nonlinear material parameters in a systematic way by means of local measurements with indentation tests. They showed that comparable results to the combined compression–shear tests are achieved. *Almeida et al.* [12] studied the production of LDPE foams by incorporating different proportions of post-use polyethylene (p-PE). They investigating the effect of different proportions of PE/p-PE on the foam morphology. The research points out that the compositions with p-PE gave an increase in the amount of cells with smaller sizes and smaller areas compared to the composition with virgin LDPE only. Additionaly, the process itself was also investigated to improve its performance. *Jahani et al.* [13] proposed a conventional foam injection-moulding process equipped with mould opening and gas counter-pressure techniques to produce relatively low-density open-cell foams. The research outcomes are the improvement of the range of achievable void fractions and cell densities with respect to the traditional process. *Heim and Tromm* [14] studied a special mould technology to produce components with locally graded foam structures and locally different densities. The process uses a precision mould opening method in which the cavity is first volumetrically filled with melt containing blowing agent. Then a short delay time is used to develop a compact skin layer, and finally the entire cavity is opened to a pre-defined extent. *Ameli et al.* [15] investigated the variation of the void fraction of PLA and PLA composite foams by using low and high pressure foaming injection moulding processes. The research points out that a high fraction void can be achieved with the low pressure process while a high fraction void is the result of the high pressure process coupled to mould opening and gas counter pressure system. *Ahmadzai et al.* [16] studied a visual observation of foaming phenomenon during processing, with the objective to evaluate the effectiveness of the mould design. The authors present a specially designed mould able to evaluate the counter-pressure and mould opening phenomena to enhance foam expansion. The main result is that the part thickness is the most influencing factor on expansion ratio and cell morphology. *Bociaga and Palutkiewicz* [17] investigated the influence of injection moulding parameters and blowing agent content on selected properties of HDPE moulded parts. The results show that the mould temperature is the main influencing factor on the properties and surface state of foamed parts. The increase of the mould temperature causes an increase of weight, density and mechanical properties. *Lopez-Gil et al.* [18] proposed an improved compression moulding process to vary density and cellular structure independently, producing tailored cellular polymers. The main feature of this process is the use of self-expandable moulds which implies cthe ontrol of the final expansion ratio by mechanical means.

The analysis of the above literature points out that the material-product-process relationship is very critical in foam injection moulding. The correct formulation of the material blend, the measurements of the main material properties, the design of the mould and process are strictly related. For this reason the experimental procedure must be accurately tuned since it is the initial step.

3. Experimental procedure

The framework used for the technological material characterization of foam injection moulding is divided into several tasks, useful to investigate materials and process formulated blends on a special injection moulding machine.

3.1 DSC analyses

The commercially available injection moulding grades of LDPE, HDPE and EVA were supplied in pellets from ExxonMobil Chemical (Irving, TX, United States) whereas two types of ADC ($C_2H_4O_2N_4$) were supplied from Rifra Mastebatches SpA (Molinetto di Mazzano, BS, Italia). The properties of the pure materials in terms of density and melt flow index are reported in Table 1.

- - - *Table 1: Material properties* - - -

A DSC 403 F3 Pegasus (Netzsch-Gerätebau GmbH, Selb, Germany), equipped with a Rhodium Furnace (sensor type S) and a DSC head (sensor types E), was used to perform kinetic analyses in the temperature range between 25 and 250 °C. The material (average weight of about 7.0 mg) was put into a standard aluminum pan (99.5% of Al, maximum dimension of ∅ 6.7 mm with a volume of 85 µl) and crimped with a manually perforated aluminum lid. An empty crimped aluminium pan has been used as reference. All measurements were carried out in the non-isothermal mode with a heating and cooling rate of 10 K/min, using nitrogen (50 ml/min) as purge gas and performing two consecutive runs per sample. Figure 1 reports the thermal cycle adopted for all DSC analyses.

- - - *Figure 1* - - -

Figure 2 - 4 show the DSC measurements of the pure materials. The melt peak temperatures of all materials during the first run are reported in Table 1.

- - - *Figure 2* - - -

- - - *Figure 3* - - -

- - - *Figure 4* - - -

The non-cross-linked EVA presents a broad plateau between 50 and 80 °C, with a maximum at 56.4 °C. The peak melt temperature of the LDPE 600 and 654 are identified at 101.3 and 108.1 °C. The difference of about 7 °C might depend on the chain length and lamellae size. The peak melt temperature of the HDPE is 145.6 °C. The results of PE show that the higher the density, the higher the peak temperature and the larger the melting heat. The two types of ADC present different DSC curves. The peaks of the first run are the decomposition steps of ADC in which solids (urazol and hydrazodicarbonamide) and a gaseous mixture of nitrogen, carbon monoxide, cyanic acid and ammonia occur, in agreement to *Bhatti et al.* [19]. About 200-210 ml of gas mixture is released per gram of ADC. For the ADC type 1 three peaks were detected at 104.7, 173.4 and 235.7 °C during the first run, while only one remains at 103.9 °C. As the second run shows, the reaction is irreversible. The ADC type 2 presents only two peaks at 106.0 and 169.2 °C during the first run and only one at 105.3 °C during the second run. Also in this case, the reaction is irreversible. The

reaction of the ADC type 2 was constrained below 200 °C by adding metal compounds such as lead and zinc stabilizers, according to results of *Robledo-Ortiz et al.* [20]. The most important reaction associated to the expanding activation occurs at 173.4 °C for the ADC type 1 and 169.2 °C for the ADC type 2.

All materials (PE, EVA) were compounded using a single-screw extruder with a degassing system and screw with a diameter of 40 mm. The weight percentages of the base materials were 70/20/10 for LDPE, EVA and HDPE. The expected melt flow index and density of the blend were 35.2 g/(10 min) and 0.930 kg/cm^3 respectively. These values, intermediate between those of LDPE and HDPE, were chosen to achieve an easy processing and a good mechanical strength. For these reasons, two PE grades with different melt flow indices, densities and chain lengths were used. The addition of EVA was necessary to give specific characteristics to the final product such as a better adhesion or capability to be easy painted. The ADC was added to the blend during mixing, with a weight percentage of 4% of the total weight of the mixture. Figure 5 shows the DSC measurements of the blend and Figure 6 of the mechanical powder mix. This mix was obtained by pulverizing base materials to the final maximum size less than 40 µm with an Ultra Centrifugal Mill ZM200 (Retsch Technology GmbH, Haan, Gemany), avoiding thermal degradation by using liquid nitrogen during processing.

- - - *Figure 5* - - -

- - - *Figure 6* - - -

Multiple main peaks can be identified in the blend due to the presence of EVA (45.6, 65.0 and 72.5 °C), LDPE (109.5 °C) and HDPE (132.2 °C). The EVA shows three peaks shifted towards higher temperatures because the copolymer is partially cross-linked due to the blending. The LDPE peak is intermediate between the two grades of LDPE due to the mixing. The HDPE is shifted towards lower temperatures because of the partial breaking of the long chains into smaller ones, the growth of the lamellae size and the co-crystallization, as *Minick et al.* [21] and *Chen et al.* [22] report. In addition the blend is sensible to the thermal treatment, as the DSC results of the second run point out. The EVA peaks disappear and the area under the LDPE peak becomes smoother due to a dilution process. The peaks in the mechanical mix are detected more clearly. In this case, only three main peaks can be identified due to the presence of EVA (74.3 °C), LDPE (112.5 °C) and HDPE (135.6 °C). Similar considerations of those made on the blend can be done on the peak melt temperatures. In addition the mix is not sensible to the thermal treatment, as the DSC measurements of the second run point out, because the peaks have quite the same values and the curve has the same shape.

3.2 Rotational rheometer analyses

The viscosity was measured by using an HAAKE MARS III rotational rheometer (Thermo Fisher Scientific Inc, Waltham, USA) in a plate-plate configuration (diameter equal to 25 mm) under nitrogen atmosphere (60 ml/minute). The device is equipped with electrically heated plates and Pyrex glass at the outer enclosure to guarantee a good temperature homogenization in the chamber. Amplitude sweep tests were initially performed to identify a stable linear viscoelastic region of the material. The amplitude was properly selected to avoid that too large strains caused a material deformation beyond the linear viscoelastic regime. If this occurs, the measurement depends on the deformation extent. For this reason, the amplitude sweep was conducted prior to the frequency sweep. Frequency sweep tests were then carried-out to measure the polymer viscosity. All measurements were performed at a set point temperature of 200 °C to face with the real process conditions. Before running tests, the gap was zeroed at this temperature and the plate gap was formerly set to 1.0 mm during all tests.

Amplitude sweep experiments were done in a strain range between 0.1% and 100%, repeating each test three times. Figure 7 reports the storage modulus G' (continuous lines) and the phase angle δ (dotted lines) in function of the strain γ of the amplitude sweep tests of the base materials, taking the average value of the three replications.

- - - *Figure 7* - - -

A stable linear region can be clearly identified for strain values between 0.1% and 1.0%. For this reason, the following frequency sweep tests were realized with a strain value equal to 0.5% for all materials, including blend and mechanical mix. The range of the strain rate was set between 0.1 and 10 1/s. Figure 8 reports the viscosity measurements of the pure materials. These measurements are in good agreement with the melt flow indexes declared by the material supplier and reported in the previous Table 2.

- - - *Figure 8* - - -

The viscosities of EVA and LDPE 600 BA are very close, while the LDPE 654 and HDPE are respectively characterized by lower and higher values. The composition of the blend and mechanical mix are designed to maintain the viscosity in the range of LDPE 600 BA and/or EVA. EVA normally presents a high viscosity for injection moulding and this requires the application of high hydraulic pressures. The addition of PE provides a higher rigidity to the products and simultaneously improves the flowability of the melt during processing, as *Iannaccone et al.* [23] report. The viscosity and melt strength of LDPE decline dramatically as the temperature increases, thus facilitating cell rupture and gas escape. The increase of the EVA content in the LDPE foaming system and crosslinking reaction is used to improve the melt viscoelasticity of LDPEand to form closed cells for a continuous foaming process, as shown by *Wang et al.* [24]. The related measurements are shown overlaid with base material results. The viscosity of the mix is higher than the viscosity of EVA which is taken as reference material. This points out that the addition of HDPE reduces the fluidity of the mix. The viscosity of the mix is equivalent to EVA, denoting that the influence of HDPE on the blend is less important, probably due to the mixing process in the extruder. In addition for given PE and EVA, the interfacial interaction in PE-rich blends is higher than EVA-rich blends, which in turn led to finer and well-distributed morphology in PE-rich blends, as reported by *Faker et al.* [25].

3.3 Foam injection moulding

A specialized 60-ton rotary injection moulding machines (Roto F 15 E) with 15 stations (Presma SpA, Varese, Italy) a 62-mm diameter screw (L/D ratio equal to 21) and a special injection system was used. The position of the injection system is fixed whereas several moulds mounted on a mould table rotate in a carousel system. Each mould consists of two shaped cavities connected with side gates and a double hot runner system. The multi-station configuration improves process efficiency because a new part is injected while the previous mould starts cooling. Moulds with different shapes and parts with different processing parameters can be used concurrently. The injection moulding machine is also equipped with an efficient shut-off nozzle, a control system of the melt pressure during holding and an injection system with a high pressure nitrogen booster. A delay time between two consecutive shots is used to avoid the polymer expansion in the sprue. The cooling time is a function of the delay time and carousel rotation. Compared to a traditional foam injection machine with a single mould system, the process lead time of this multi-station system is significantly reduced. The blend/ADC mixture is injected into the mould cavities and the foaming process directly starts inside the mould. Figure 9 shows the main steps of the foam injection moulding, together with the machine scheme. The process parameters are reported in Table 2.

- - - *Figure 9* - - -

- - - *Table 2* - - -

The temperatures of the three sections of the heater band were linearly increased from 185 °C to the injection temperature equal to 200 °C. The process parameters were kept constant for all production runs. Two types of mixtures (blend and mechanical mix) combined with two types of ADC were used during the production, as Table 3 reports. The minimum quantity of each mixture used during production runs was equal to 500 kg.

- - - *Table 3* - - -

A full cleaning of the hopper and screw was done before using a new mixture. As soon as the process reaches stationary conditions, the parts were collected. No stop events occurred during the production run.

4. Results

The visual analysis was performed to assess the quality of the foam injected parts. The presence of visual defects (cracking, crazing, grooves, ripples, wave marks, etc.) is aesthetically not permitted. These defects are also considered as performance defects because they are an indication of part failure resulting from internal and external stresses exceeding the strength of the part due to bubble formation or presence of too large bubbles. If the part did not meet the expectations, the cause of the problem was classified and identified. Obviously the most common causes of these visual defects depend on the material and/or process. The visual inspection was initially carried-out on the entire part and then on specific sections, considered as critical areas of interest. Sections were taken from the moulded parts by cutting them with a diamond cut-off wheel and grinding with several SiC foils (grit size FEPA P from 120 to 4,000). Figure 10 shows the sections of parts obtained after processing blend and mechanical mix with the two types of ADC. The part color was initially analyzed in the visual inspection procedure to evaluate the material-process interaction. The color of the part made with the PE/EVA blend and ADC type 1 (Part #1) is white changing to grey while the part with the PE/EVA mix and ADC type 1 (Part #2) is white with some yellow areas. These yellow areas are an important evidence of incomplete reactions of the ADC type 1, because the color of the foaming agent is yellow. The parts realized with the ADC type 2 are both fully white and no color variations are detected. However, from the direct inspection, it is not possible to evaluate the complete reaction of the foaming agent because its color is white. Thus, an evaluation of the pore distribution and dimensions was performed, in terms of average diameter value and standard deviation (Table 4). The porosity of Part #1 is higher and less uniformly distributed than Part #2, with presence of several large pores in the core (average diameter greater than 2000 μm). This condition is considered as unacceptable due to the expected lower strength. As concern Part #3 and #4, the pores are uniformly distributed but the dimensions are higher than the ones of Part #1. Small and densely spaced pores were obtained. This can be explained by the lower activation temperature of the foaming agent and the longer solidification time. The gas bubbles are linked together in a liquid polymer and the plastic solidifies more quickly, which is limiting the growth of the gas bubbles.

- - - *Table 4* - - -

The DSC analysis was carried-out for the quantitative analysis, selecting two specific points of interest, located in the core and at the surface of the part and subject to the same thermal cycle imposed to the base materials. The DSC curves of the PE/EVA blend (Figure 11 - a and b) and PE/EVA mix (Figure 11 - c and d) are quite similar in the first run and become equal in the second run, after the thermo-mechanical history induced by the process was destroyed. The DSC curves present

two peaks associated to the LDPE and HDPE. The difference between the surface and core DSC curves of both parts are justified considering that the surface cannot expand due to the rapid cooling while very slow cooling conditions in the core promotes the free expansion. In particular the crystallization degree of LDPE is higher in the core and lower at the skin layer, while no appreciable variations with the HDPE are recorded. The part with the PE/EVA blend is lighter, with a weight reduction of about 3.9% compared to the part with the PE/EVA mix. Particular interesting is the identification of a very small peak at 167.2 °C in the DSC measurements of the PE/EVA blend form the surface which reveals that some residuals of ADC continue to be active. Figure 12 shows the sections of parts obtained from blend and mechanical mix with the ADC type 2. The porosity of both parts is higher than the previous ones, with a high number of small pores uniformly distributed. This shows that the gas creation during the decomposition of the ADC type 2 is more efficient. The DSC analyses, performed at the surface and in the core of the parts, are subjected to the previously defined thermal cycle. Also in this case, the DSC curves of the PE/EVA blend (Figure 12 - a and b) and PE/EVA mix (Figure 12 - c and d) are quite similar in the first run and equal in the second run. No evident trace of ADC residuals is present in the parts. The crystallization degree value is higher in the core and lower at the surface, as expected. A small peak is detected around 75 °C in the DSC measurements at the surface. This peak is associated to the presence of EVA. In this case the part with the PE/EVA blend is lighter, with a weight reduction of about 2.1% compared to the part with the PE/EVA mix and 1.3% lighter than the part with PE/EVA blend and ADC type 1.

5. Conclusions

The study of the PE/EVA blends shows that good results can be achieved by accurately controlling the blend formulation and mixing as well as by correctly selecting the foaming agent. One advantage of using an ADC chemical foaming agent is that that existing equipment does not need to be modified. The chemical foaming agent is easy to compound and can be added to the PE/EVA blend in the hopper. The results points out that the use of the blend with ADC type 1 leads to a higher porosity and better coloration of the part, with a consequent reduction of the part weight. The use of a ADC type 2, characterized by a lower decomposition temperature range, allows a better pore distributions to be achieved. Further research should be addressed to numerically simulate the process and improve the part performance, evaluating crystallization and mechanical strength by using a specific design framework (*Spina et al.* [26]).

Acknowledgements

The authors wish to thank Prof. Luigi Tricarico of DMMM (Politecnico di Bari), Marcel Spekowius of IKV (RWTH Aachen University), Alfredo Vania of VANPLAST srl (Barletta) for their precious suggestions and support during the research activities. The research was partially funded by Italian National Operative Program as SMATI project (PON01_02584). The author would like to extend his thanks to the organization mentioned.

References

1. Hornsby PR. Thermoplastics structural foams: Technology of production. Materials & Design 1982; 3:354–362.
2. Liu PS, Chen GF. Producing Polymer Foams. Porous Materials 2014; 345-382.
3. Allen RD, Newman ST, Mitchell SR, Temple RI, Jones CL, Boer CR, Dulio S. Design of experiments for the qualification of EVA expansion characteristics. Robotics and Computer-Integrated Manufacturing 2005; 21:412–420.
4. Barzegari MR, Kabamba ET, Rodrigue D. Flexural modulus prediction of symmetric structural polymer foams with complex density profiles. J of Porous Materials 2011; 18:715–721.

5. Solorzano E., Rodriguez-Perez M.A., Polymeric Foams. Structural Materials and Processes in Transportation. Wiley-VCH Verlag GmbH & Co; 2013, 375–411.
6. Reyes-Labarta JA, Marcilla A. Differential scanning calorimetry analysis of the thermal treatment of ternary mixtures of ethylene vinyl acetate, polyethylene, and azodicarbonamide. J. of Applied Polymer Science 2008; 110:3217–3224.
7. Zhang X, Yang H, Song Y, Zheng Q. Influence of Crosslinking on Crystallization, Rheological, and Mechanical Behaviors of High Density Polyethylene/Ethylene-Vinyl Acetate Copolymer Blends. Polymer Engineering & Science 2014; 54:2848–2858.
8. Vachon C. Research on Alternative Blowing Agents. Thermoplastic Foam Processing: Principles and Development. CRC Press; 2008; 139–192.
9. Greco A, Maffezzoli A, Manni O. Development of polymeric foams from recycled polyethylene and recycled gypsum. Polymer Degradation and Stability 2005; 90:256–263.
10. Antunes M, Velasco JI. Multifunctional polymer foams with carbon nanoparticles. Progress in Polymer Science 2014; 39:486–509.
11. Li B, Gu YD, English R, Rothwell G, Ren XJ. Characterisation of nonlinear material parameters of foams based on indentation tests. Materials & Design 2009; 30:2708–2714.
12. Almeida MG, Demori R, Zattera AJ, Zeni M. Morphological analysis of polyethylene foams with post-use material incorporated. Polymer Bulletin 2007; 59:83–90.
13. Jahani D, Ameli A, Jung PU, Barzegari MR, Park CB, Naguib H. Open-cell cavity-integrated injection-molded acoustic polypropylene foams. Materials & Design 2014; 53:20–28.
14. Heim H-P, Tromm M. General aspects of foam injection molding using local precision mold opening technology. Polymer 2015; 56:111–118.
15. Ameli A, Jahani D, Nofar M, Jung PU, Park CB. Development of high void fraction polylactide composite foams using injection molding: Mechanical and thermal insulation properties. Composites Science and Technology 2014; 90:88–95.
16. Ahmadzai A, Behravesh AH, Sarabi MT, Shahi P. Visualization of foaming phenomena in thermoplastic injection molding process. Journal of Cellular Plastics 2014, 50:279–300.
17. Bociaga E, Palutkiewicz P. The Influence of Injection Molding Parameters and Blowing Agent Addition on Selected Properties, Surface State, and Structure of HDPE Parts. Polymer Engineering & Science 2013; 53:780–791.
18. Lopez-Gil A, Saiz-Arroyo C, Tirado J, Rodriguez-Perez MA. Production of non-crosslinked thermoplastic foams with a controlled density and a wide range of cellular structures. J. of Applied Polymer Science 2015. In press.
19. Bhatti AS, Dollimore D, Goddard RJ, O'Donnel G. The thermal decomposition of azodicarboamide. Thermochinica Acta 1984; 76:63–77.
20. Robledo-Ortiz JR, Zepeda C, Gomez C, Rodrigue D, Gonzalez-Nunez R. Non-isothermal decomposition kinetics of azodicarbonamide in high density polyethylene using a capillary rheometer. Polymer Testing 2008; 27:730–735.
21. Minick J, Moet A, Baer A. Morphology of HDPE/LDPE blends with different thermal histories. Polymer 1995; 36:1923–1932.
22. Chen Y, Zou H, Liang M, Cao Y. Melting and crystallization behavior of partially miscible high density polyethylene/ethylene vinyl acetate copolymer (HDPE/EVA) blends. Thermochimica Acta 2014; 586:1–8.
23. Iannaccone A, Amitrano S, Pantani R. Rheological and Mechanical Behavior of Ethyl Vinyl Acetate/Low Density Polyethylene Blends for Injection Molding. J. of Applied Polymer Science 2013; 127:1157–1163.

24. Wang W, Gong W, Zheng B. Improving Viscoelasticity and Rebound Resilience of Crosslinked Low-Density Polyethylene Foam by Blending With Ethylene Vinyl Acetate and Polyethylene-Octene Elastomer. J. of Vinyl and Additive Technology. In press.
25. Faker M, Razavi Aghjeh MK, Ghaffari M, Seyyedi SA. Rheology, morphology and mechanical properties of polyethylene/ethylene vinyl acetate copolymer (PE/EVA) blends. European Polymer Journal 2008; 44:1834–1842
26. Spina R, Spekowius M, Dahlmann R, Hopmann C. Analysis of polymer crystallization and residual stresses in injection molded parts. Int. J. of Precision Engineering and Manufacturing 2014; 15:89–96.

Table

Name	Material type	Density *g/cm³*	Melt flow index *g/10 min*	Melt temperature (*) *°C*
Escorene Ultra UL02528CC	EVA (25% VA)	0.951	25 g/10 min	56.4
LD 600 BA	LDPE	0.924	21 g/10 min	101.3
LD 654	LDPE	0.913	70 g/10 min	108.1
HMA 035	HDPE	0.964	8 g/10 min	145.6
ADC Type 1	ADC	0.55	-	173.4
ADC Type 2	ADC	0.55	-	169.2

*this data was experimentally obtained by the author

Table 1: DSC results - Base materials

Parameter	Value	Parameter	Value	Parameter	Value	Parameter	Value
Melt temperature	200 °C	Injection volume	220 cm^3	Holding pressure	80 MPa	Cooling time	300 s
Mold temperature	6 °C	Injection speed	60 mm/s	Holding time	6 s	Delay time	10 s

Table 2: Process parameters

ID	Materials	Compound
Part #1	EVA, LDPE, HDPE, ADC type 1	Mechanical
Part #2	EVA, LDPE, HDPE, ADC type 1	Blend
Part #3	EVA, LDPE, HDPE, ADC type 2	Mechanical
Part #4	EVA, LDPE, HDPE, ADC type 2	Blend

Table 3: Mixtures

ID	Average diameter (μm)	Standard deviation (μm)
Part #1	326	151
Part #2	553	335
Part #3	435	130
Part #4	476	145

Table 4: Pore distribution

Figure

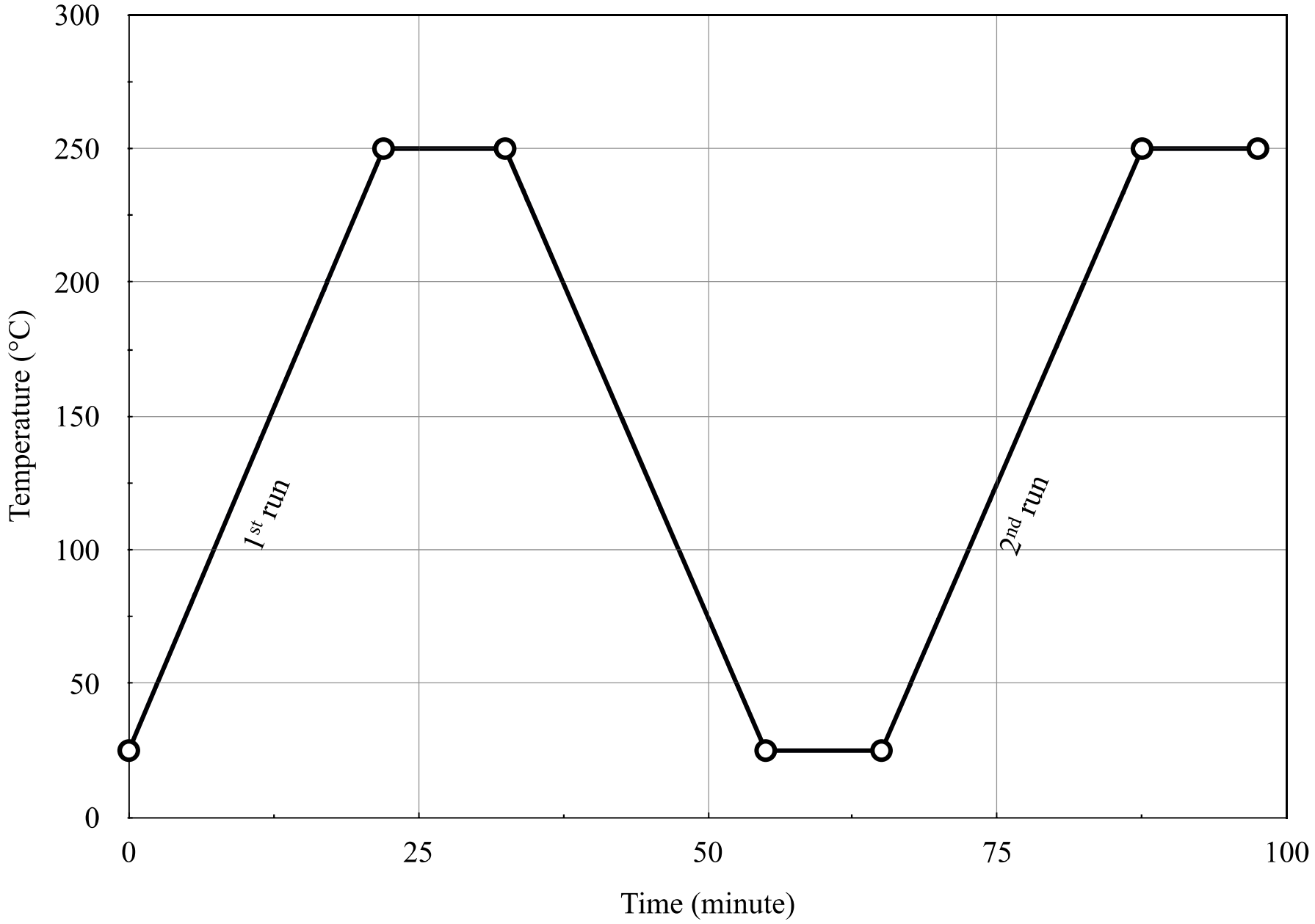

Figure 1: Thermal cycle

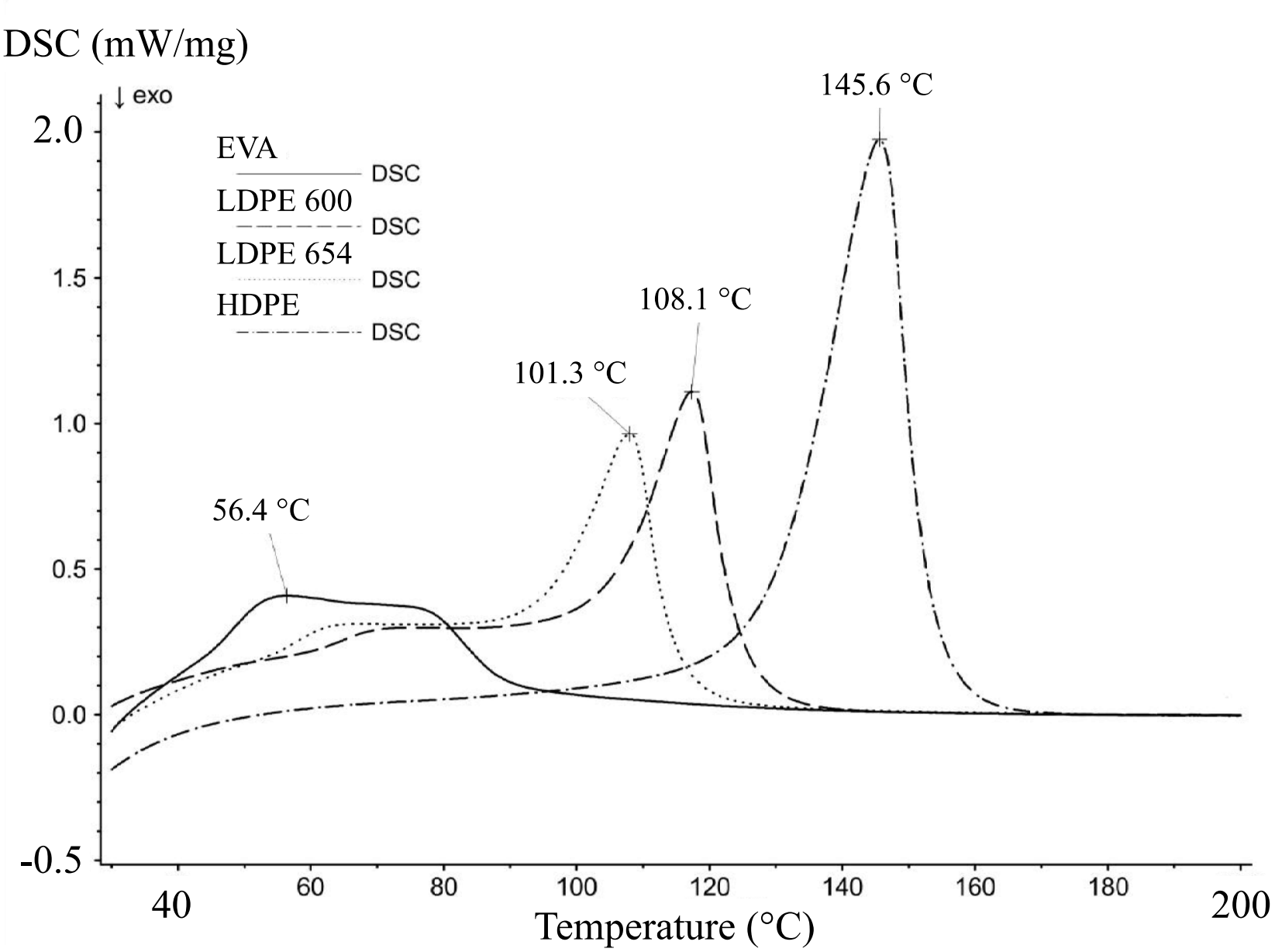

Figure 2: DSC results - Pure materials - 1st run

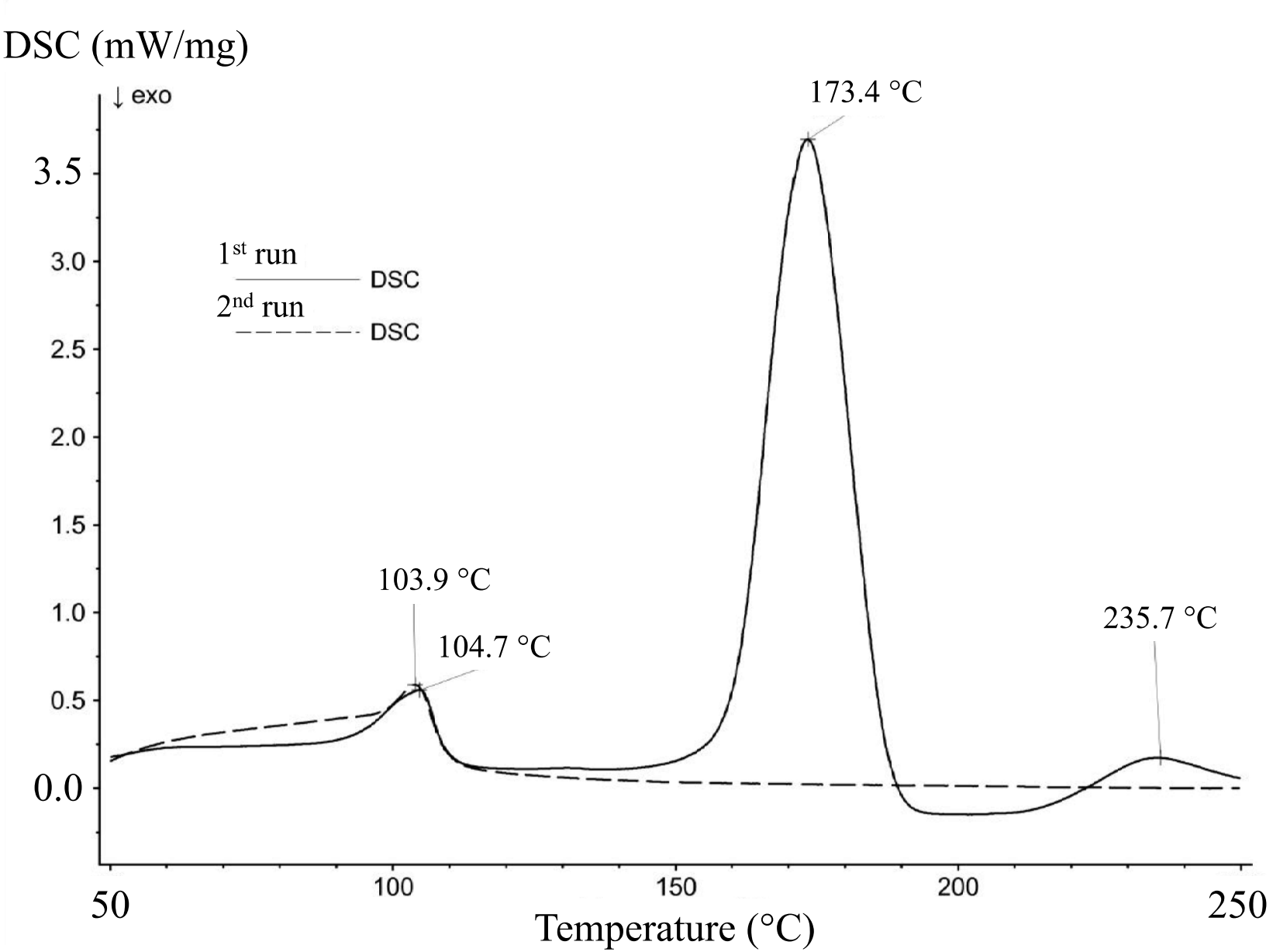

Figure 3: DSC results - ADC type 1 - 1st and 2nd run

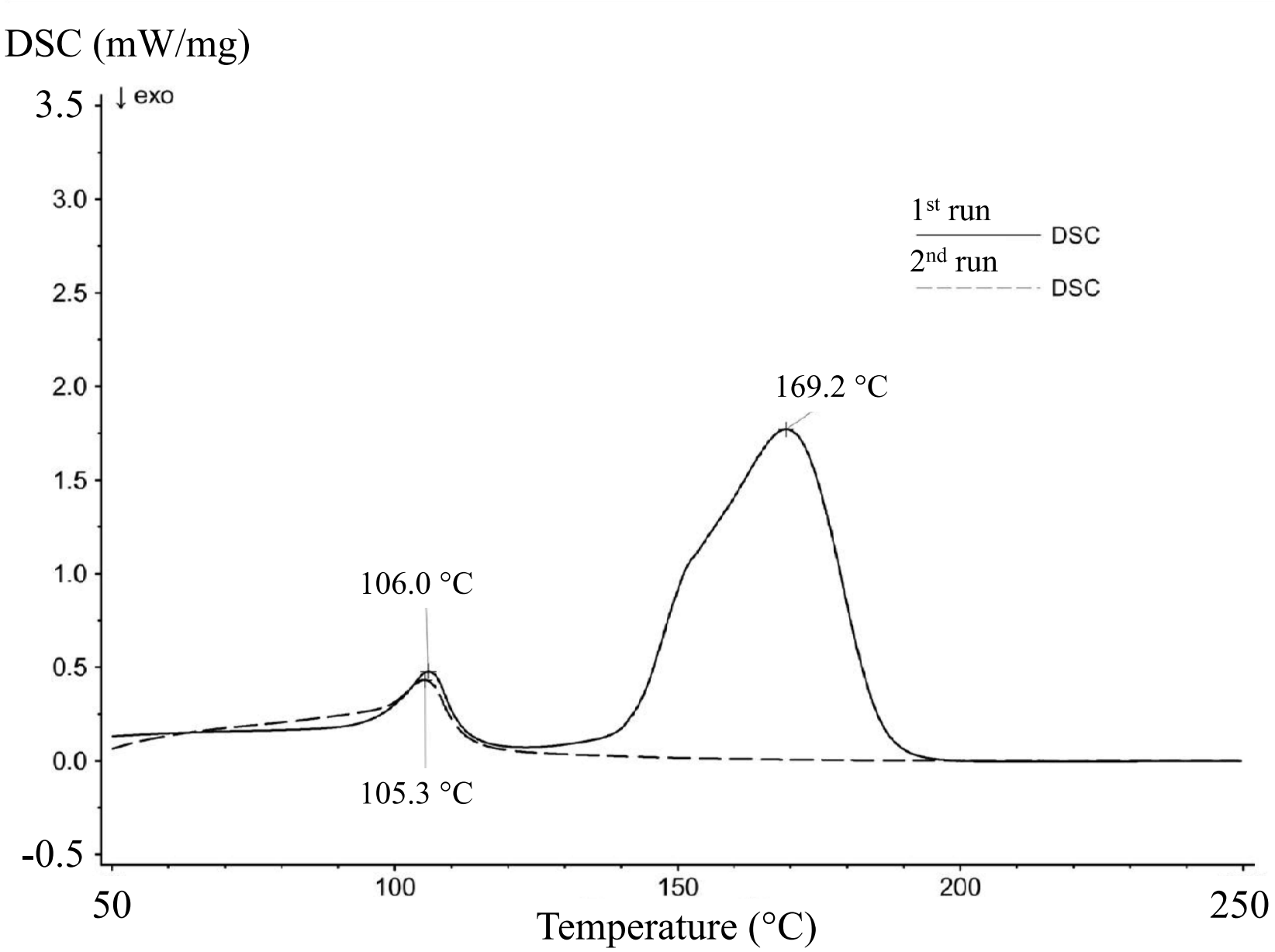

Figure 4: DSC results - ADC type 2 - 1st and 2nd run

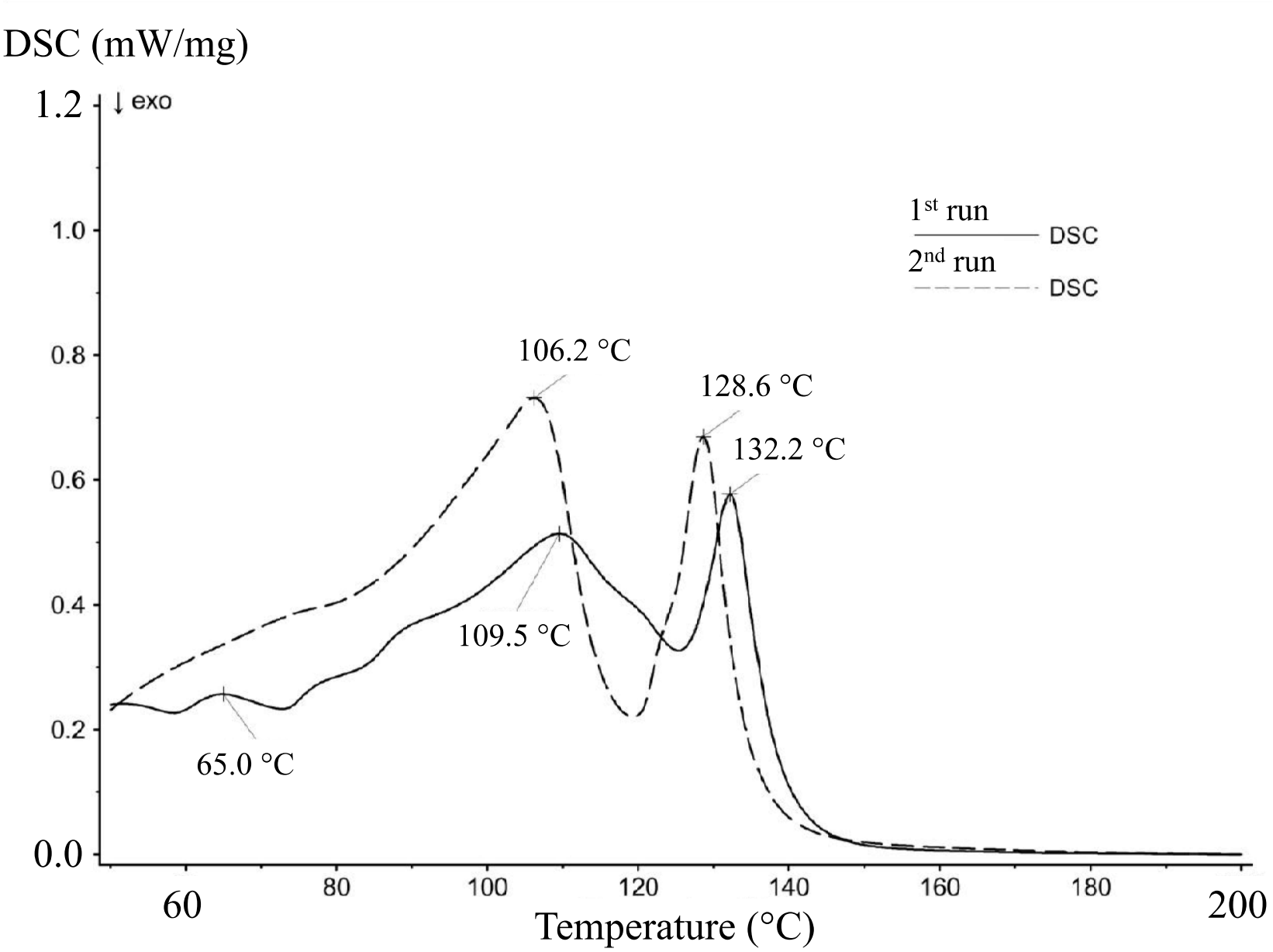

Figure 5: DSC results - Blend - 1st and 2nd run

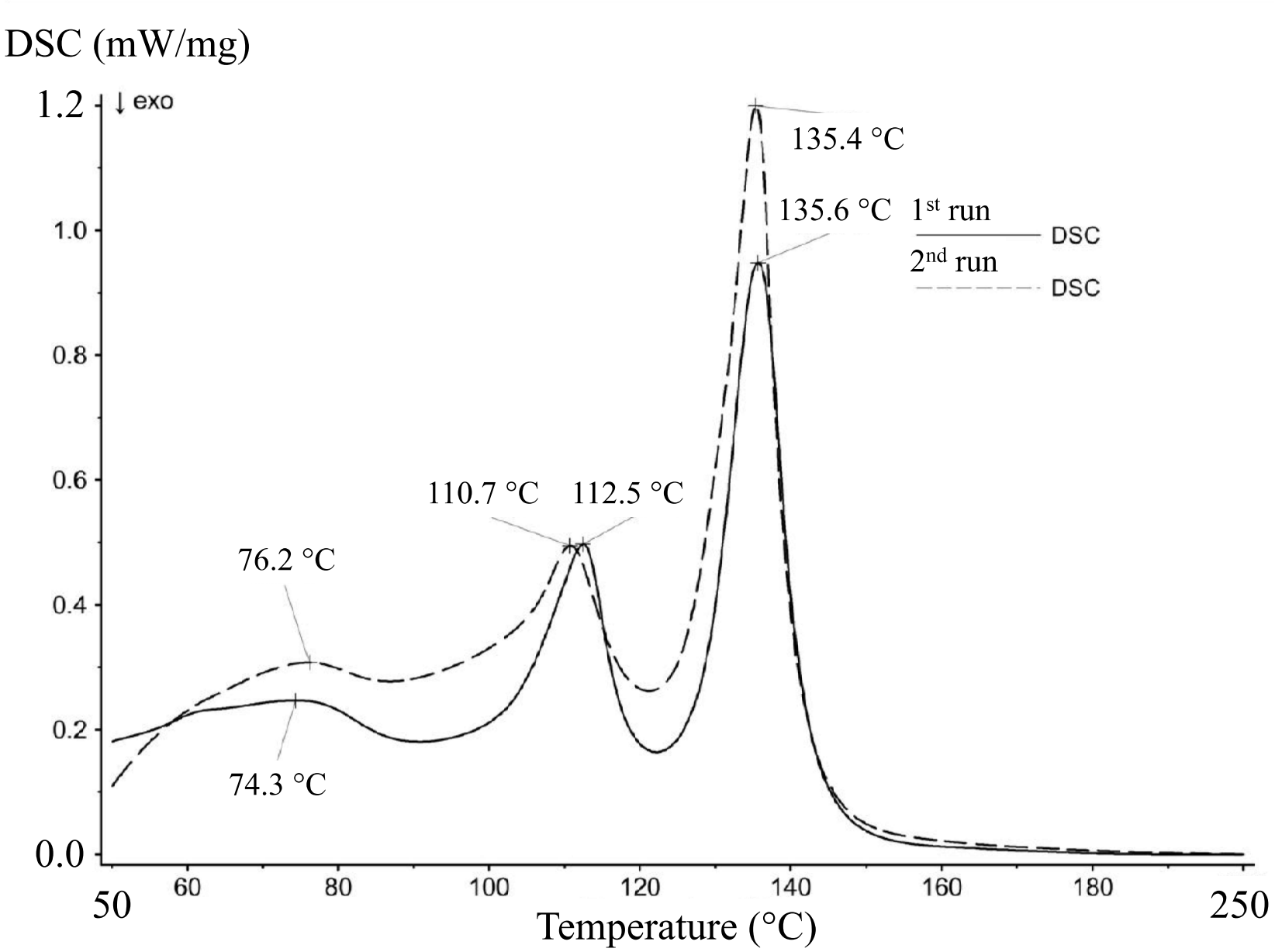

Figure 6: DSC results - Mix - 1st and 2nd run

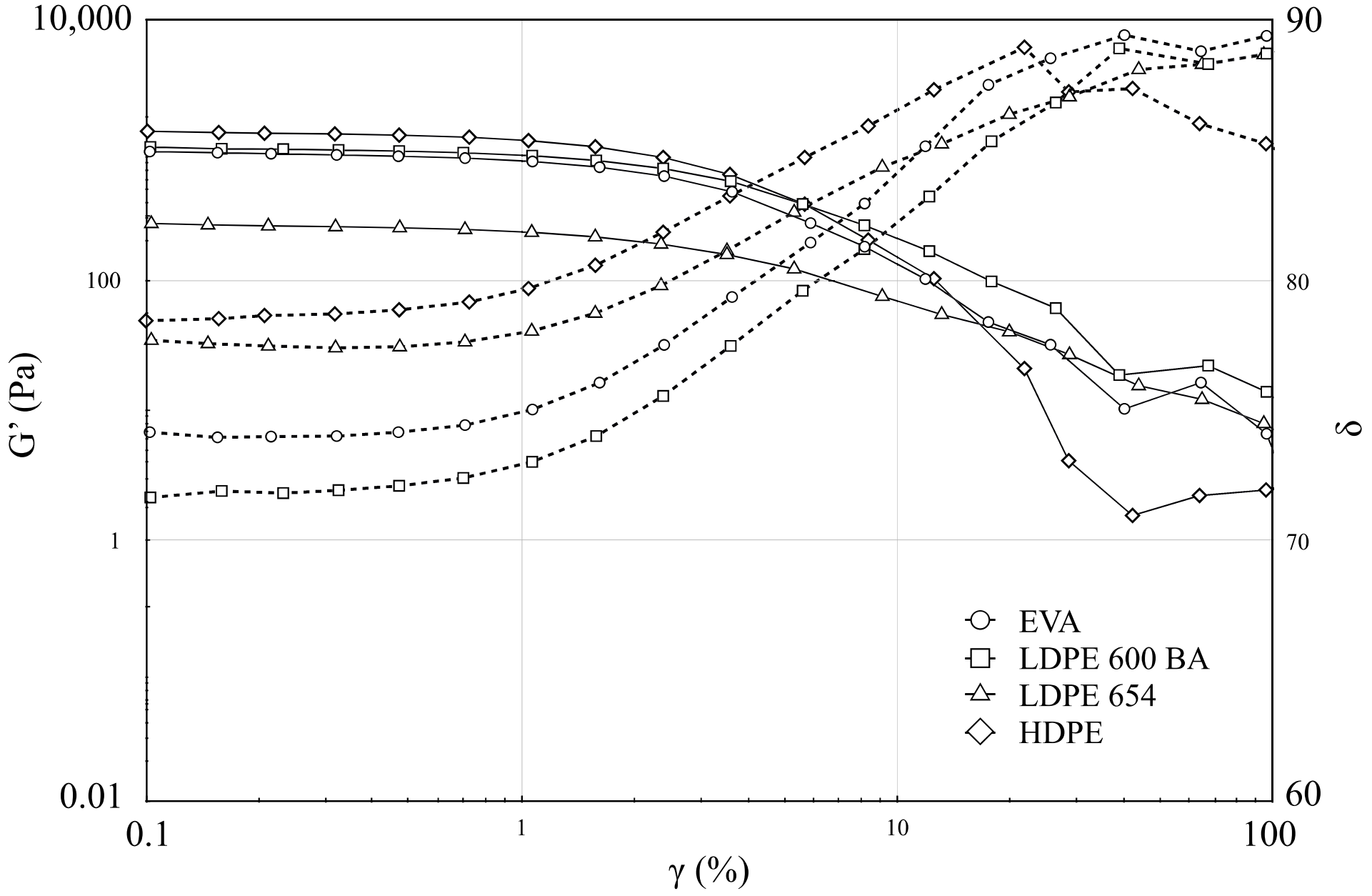

Figure 7: Rheometer results - Amplitude sweep

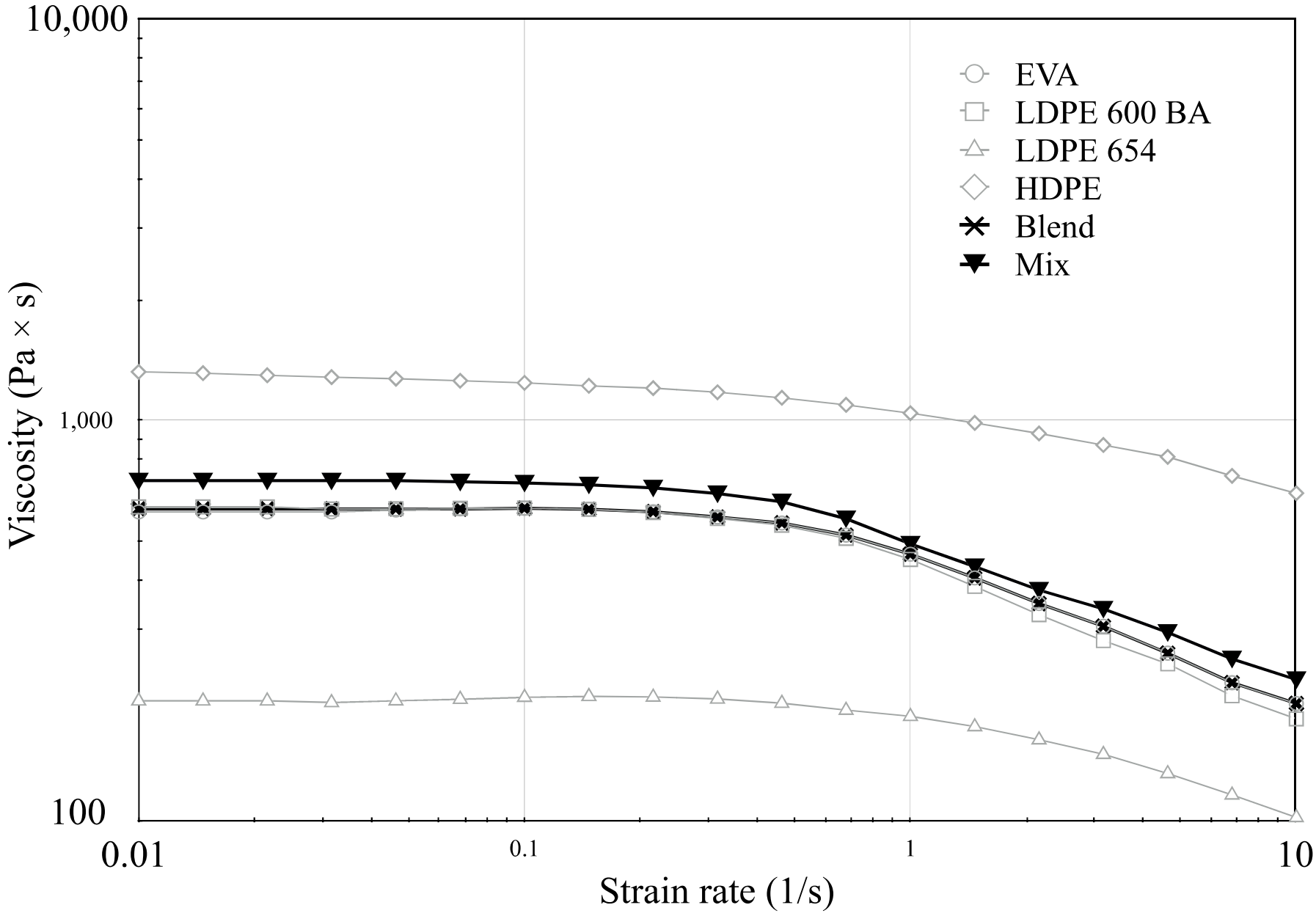

Figure 8: Rheometer results - Frequency sweep

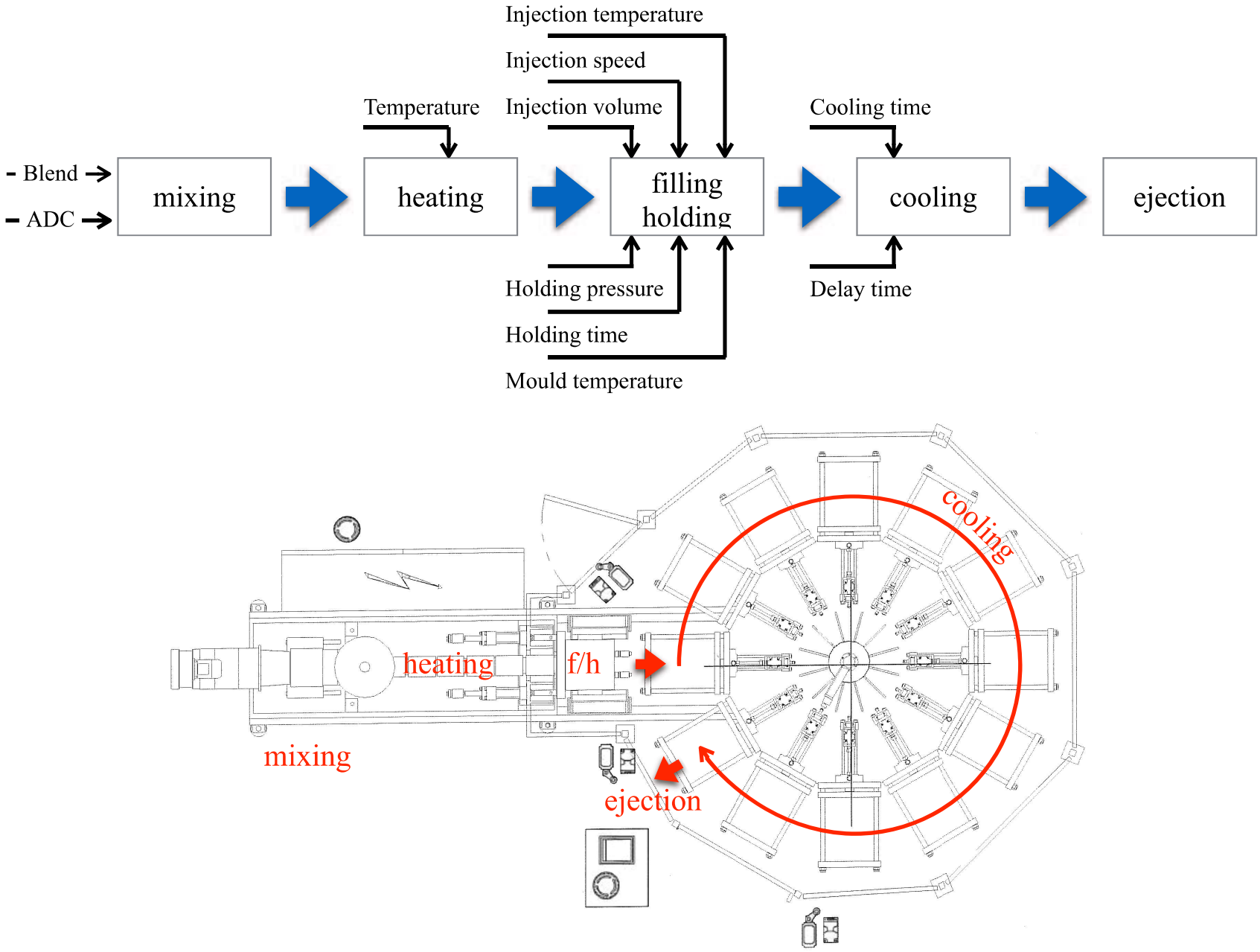

Figure 9: Process flow and machine scheme

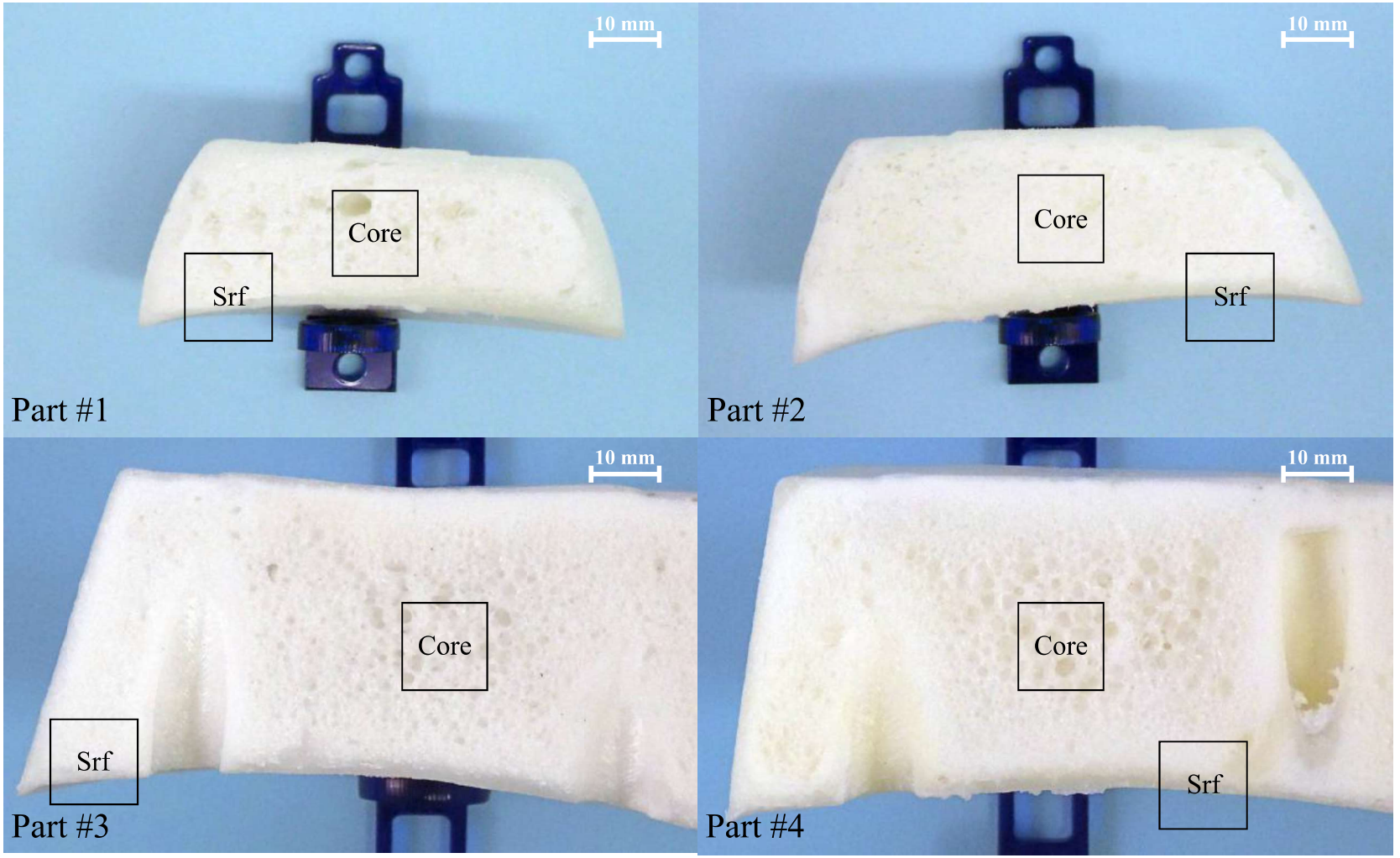

Figure 10: Moulded parts

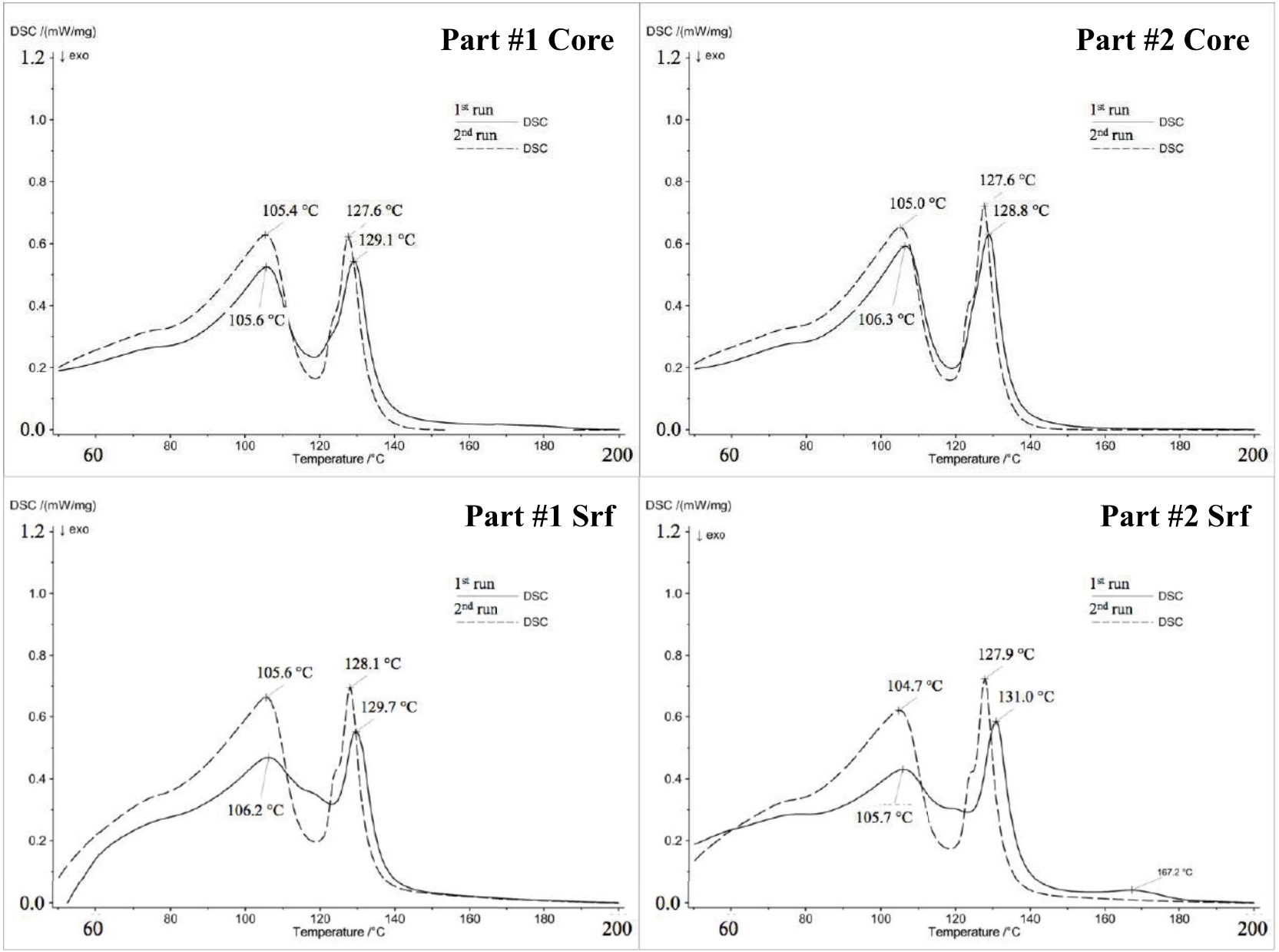

Figure 11: DSC results - Part #1 & #2 - 1st and 2nd run

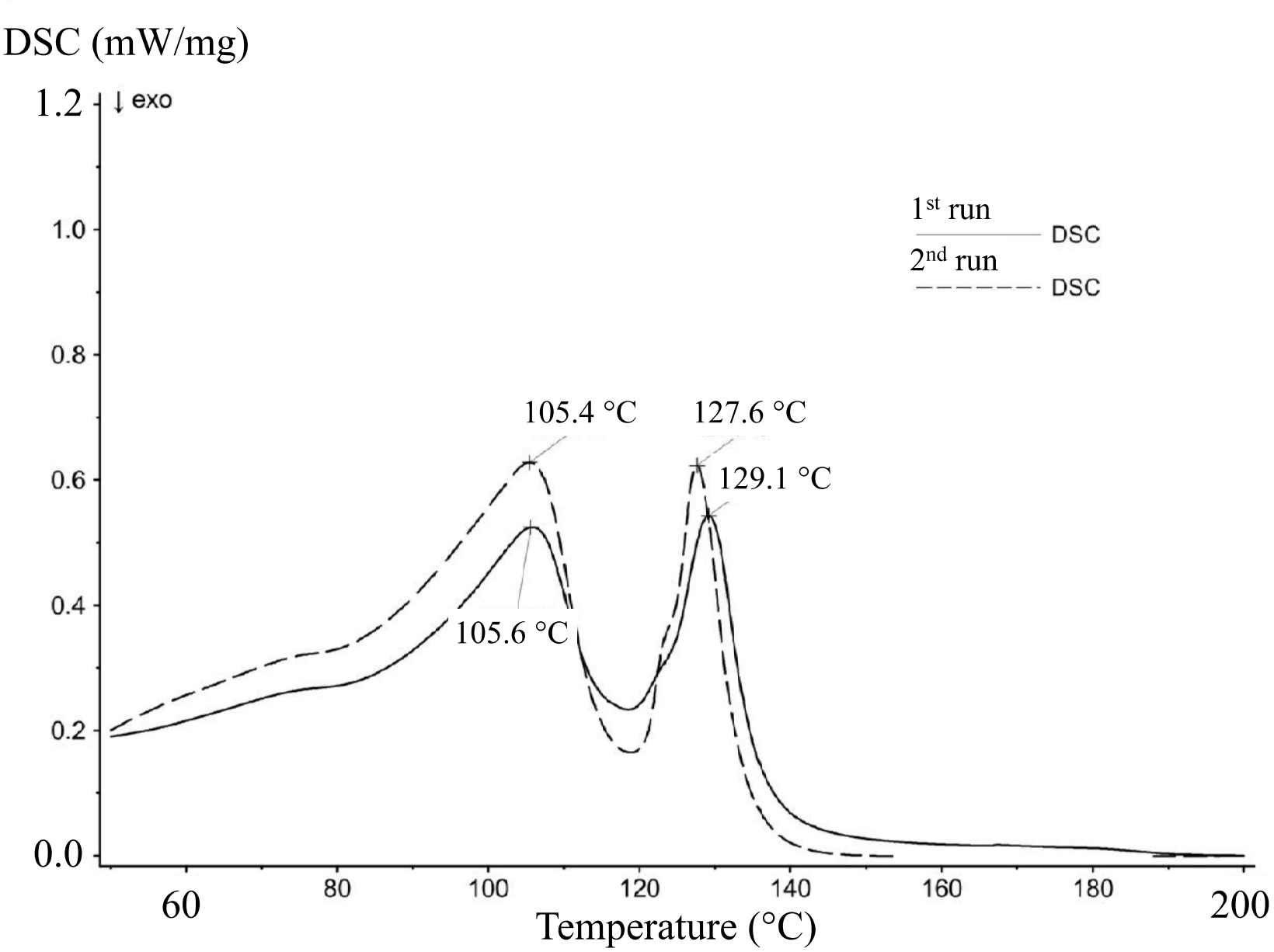

Figure 11-a: DSC results - Part #1 Core - 1st and 2nd run

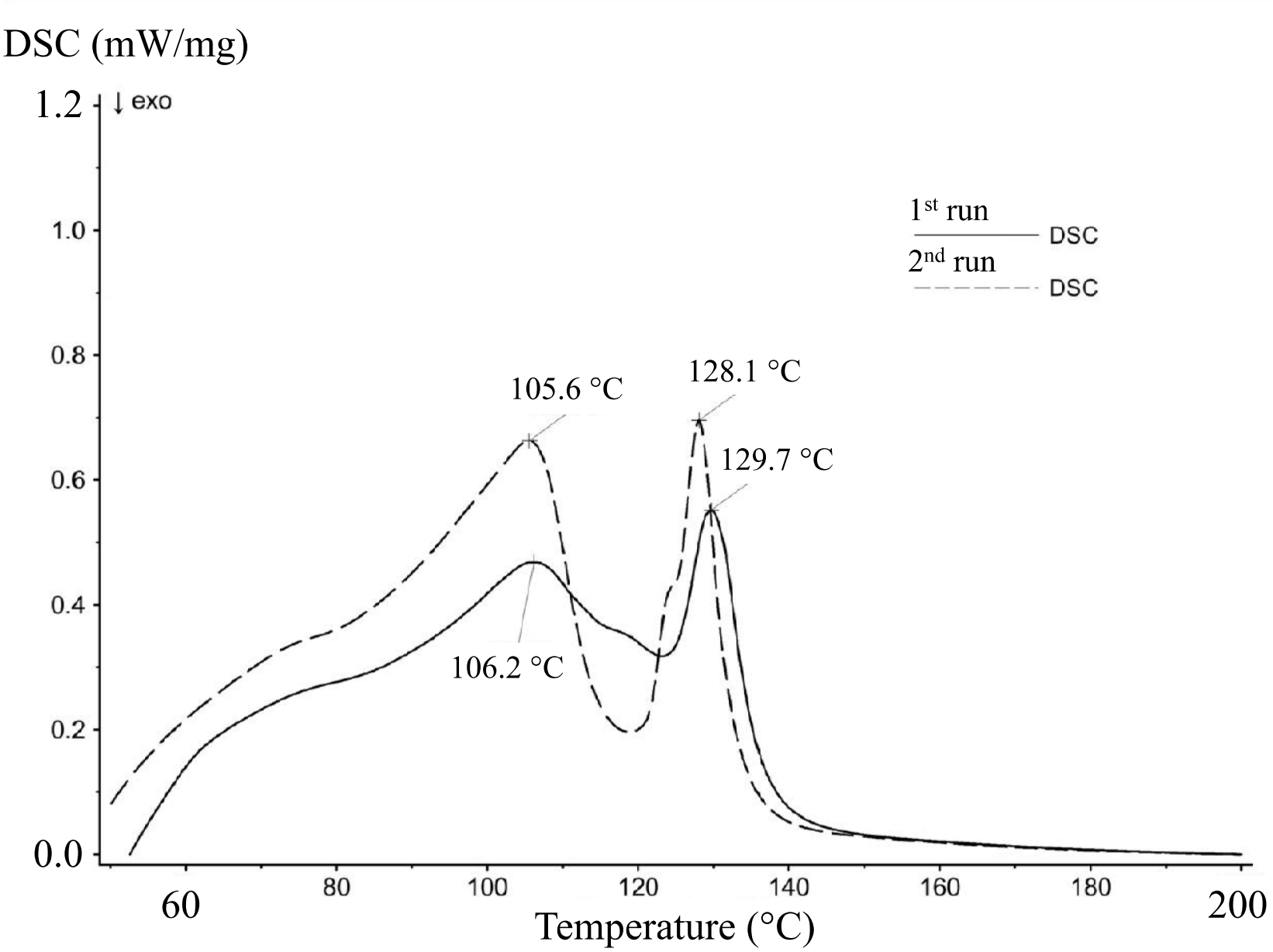

Figure 11-b: DSC results - Part #1 Srf - 1st and 2nd run

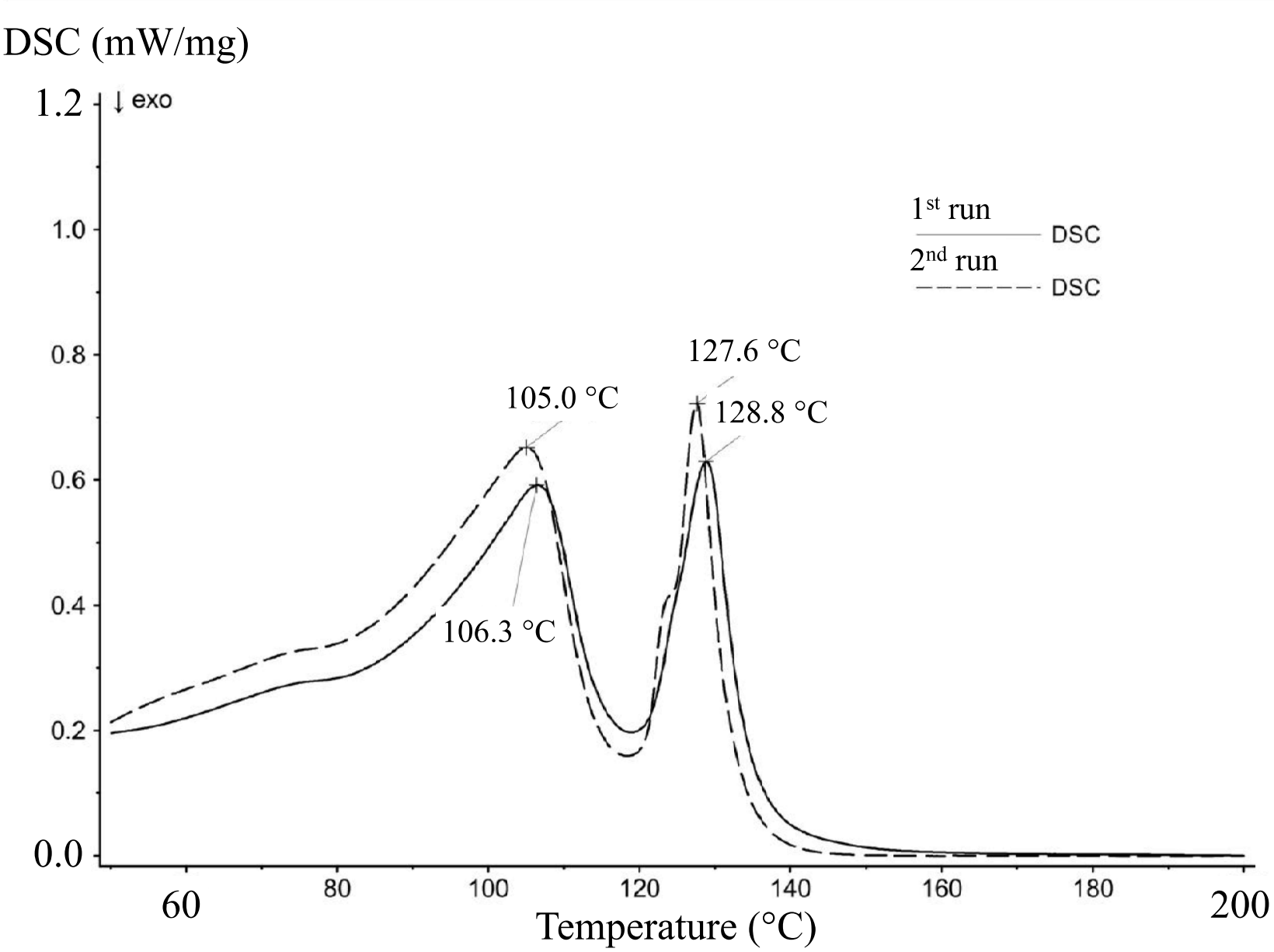

Figure 11-c: DSC results - Part #2 Core - 1st and 2nd run

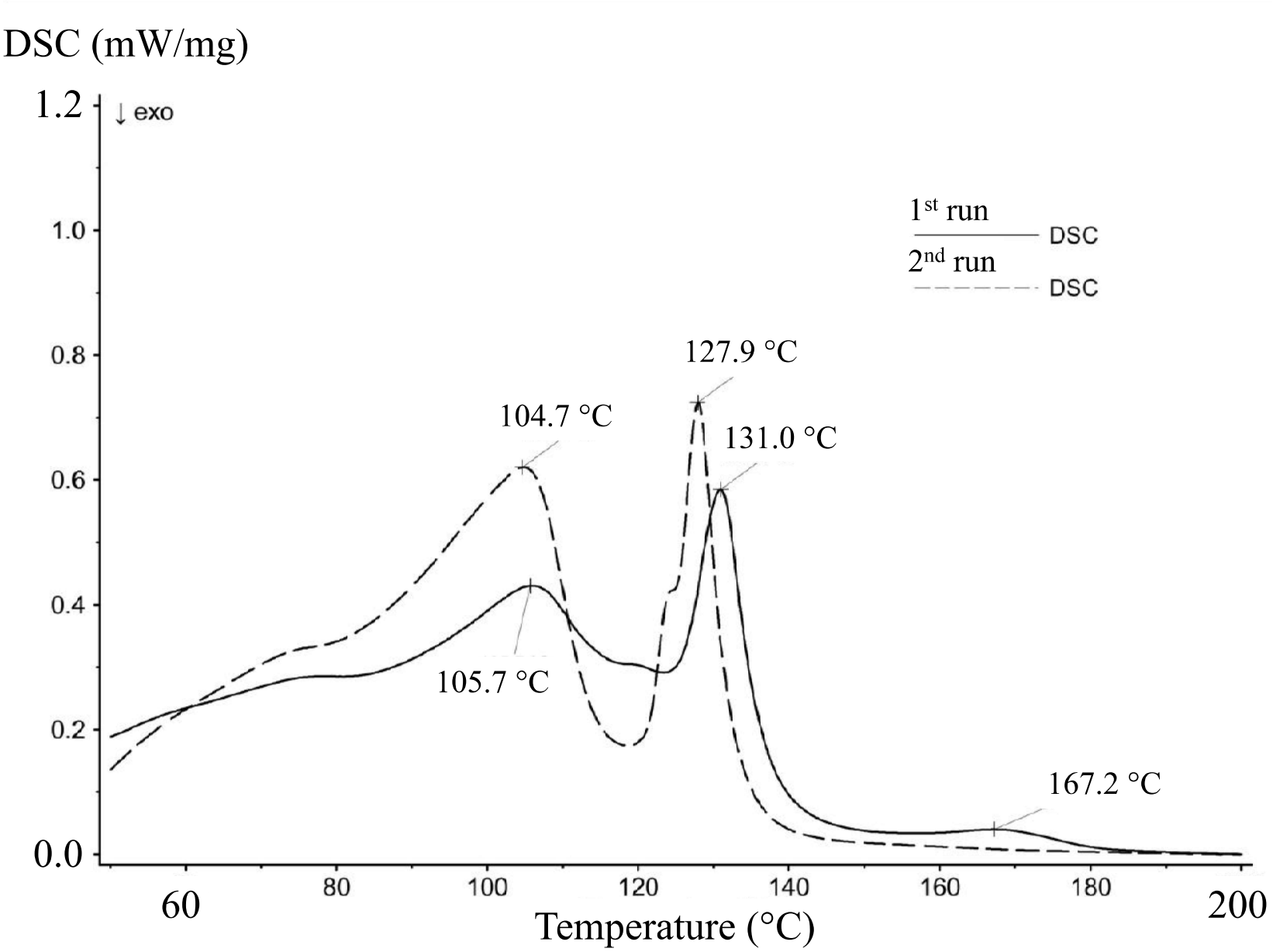

Figure 11-d: DSC results - Part #2 Srf - 1st and 2nd run

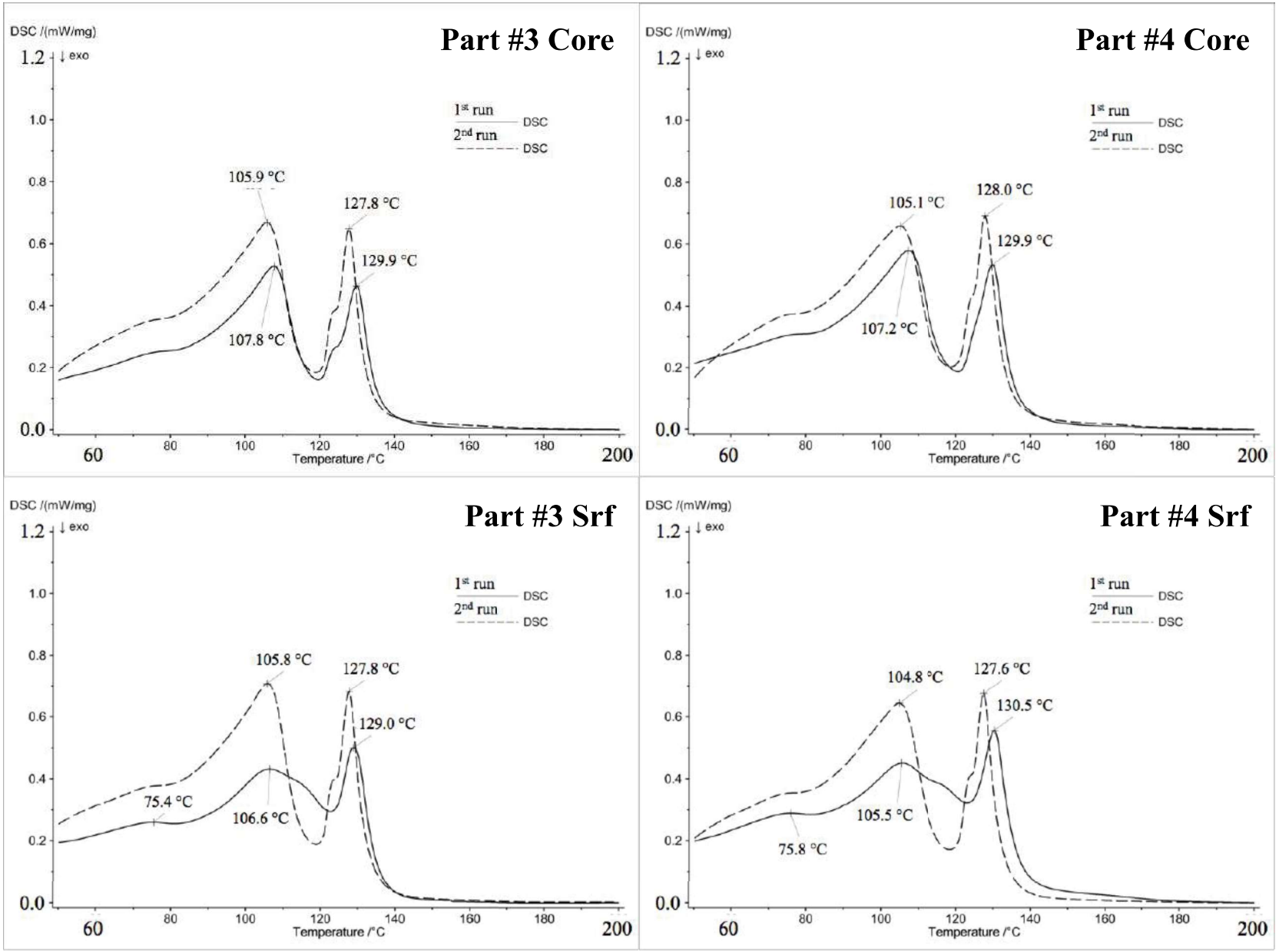

Figure 12: DSC results - Part #3 & #4 - 1st and 2nd run

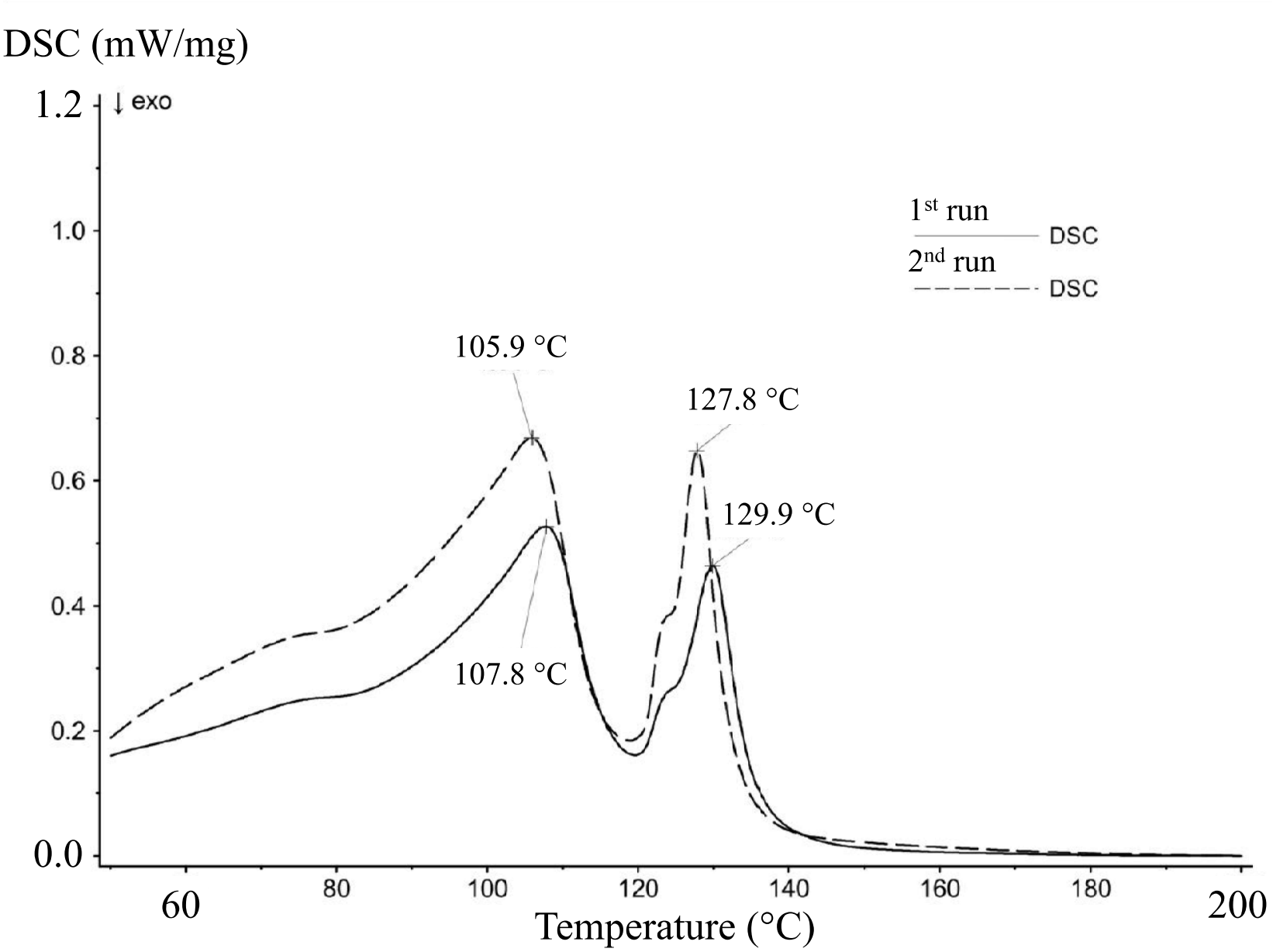

Figure 12-a: DSC results - Part #3 Core - 1st and 2nd run

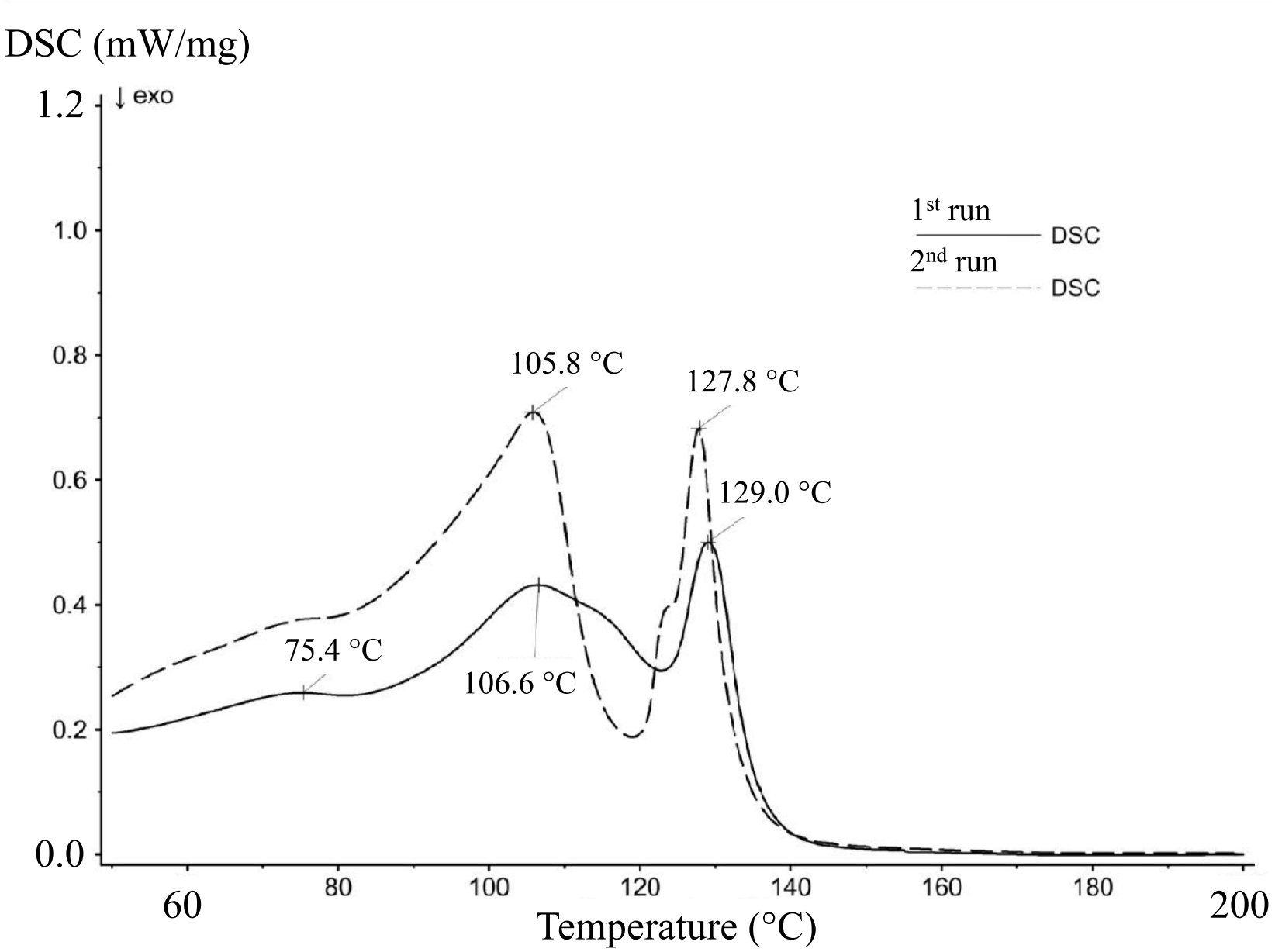

Figure 12-b: DSC results - Part #3 Srf - 1st and 2nd run

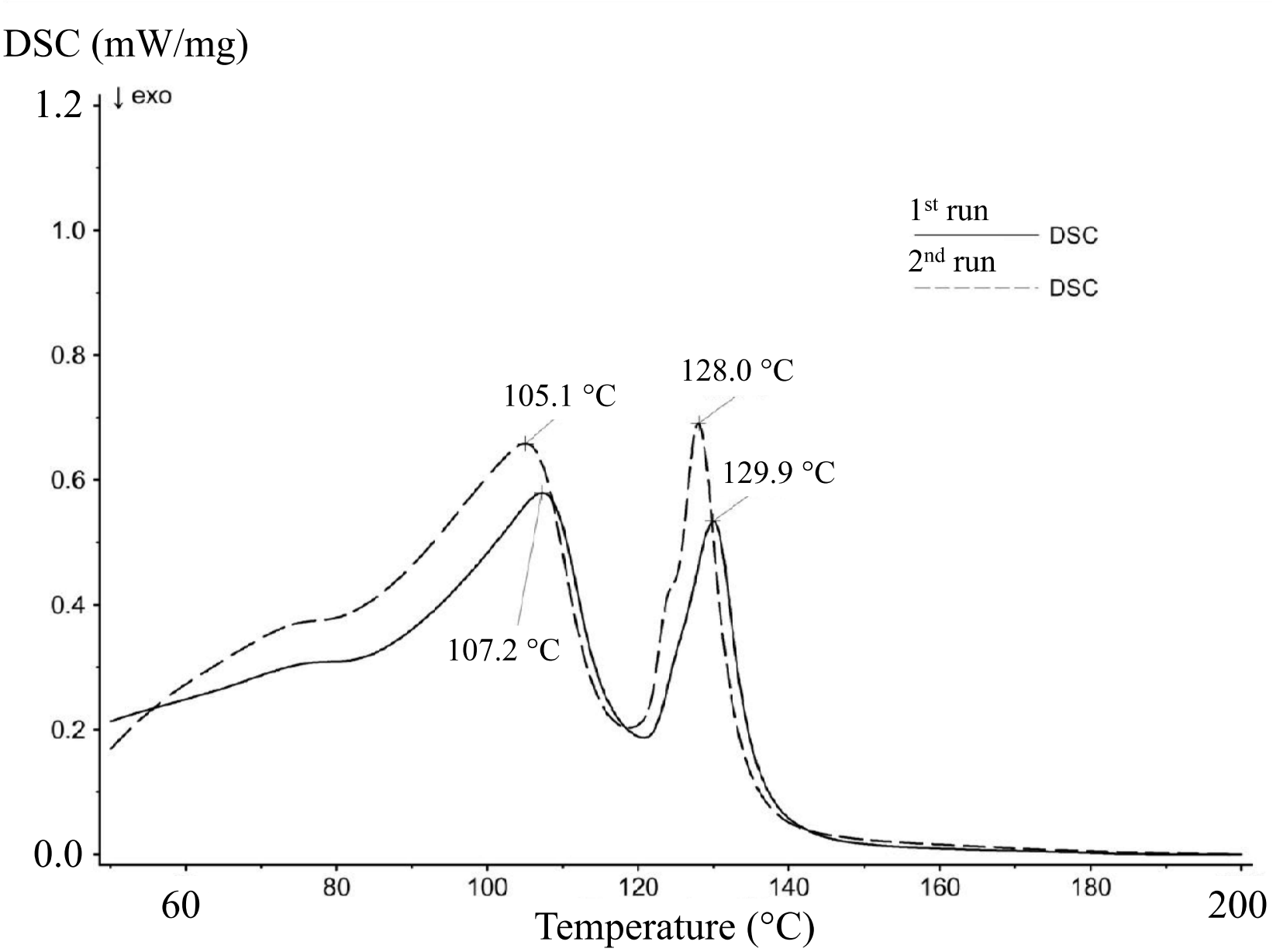

Figure 12-c: DSC results - Part #4 Core - 1st and 2nd run

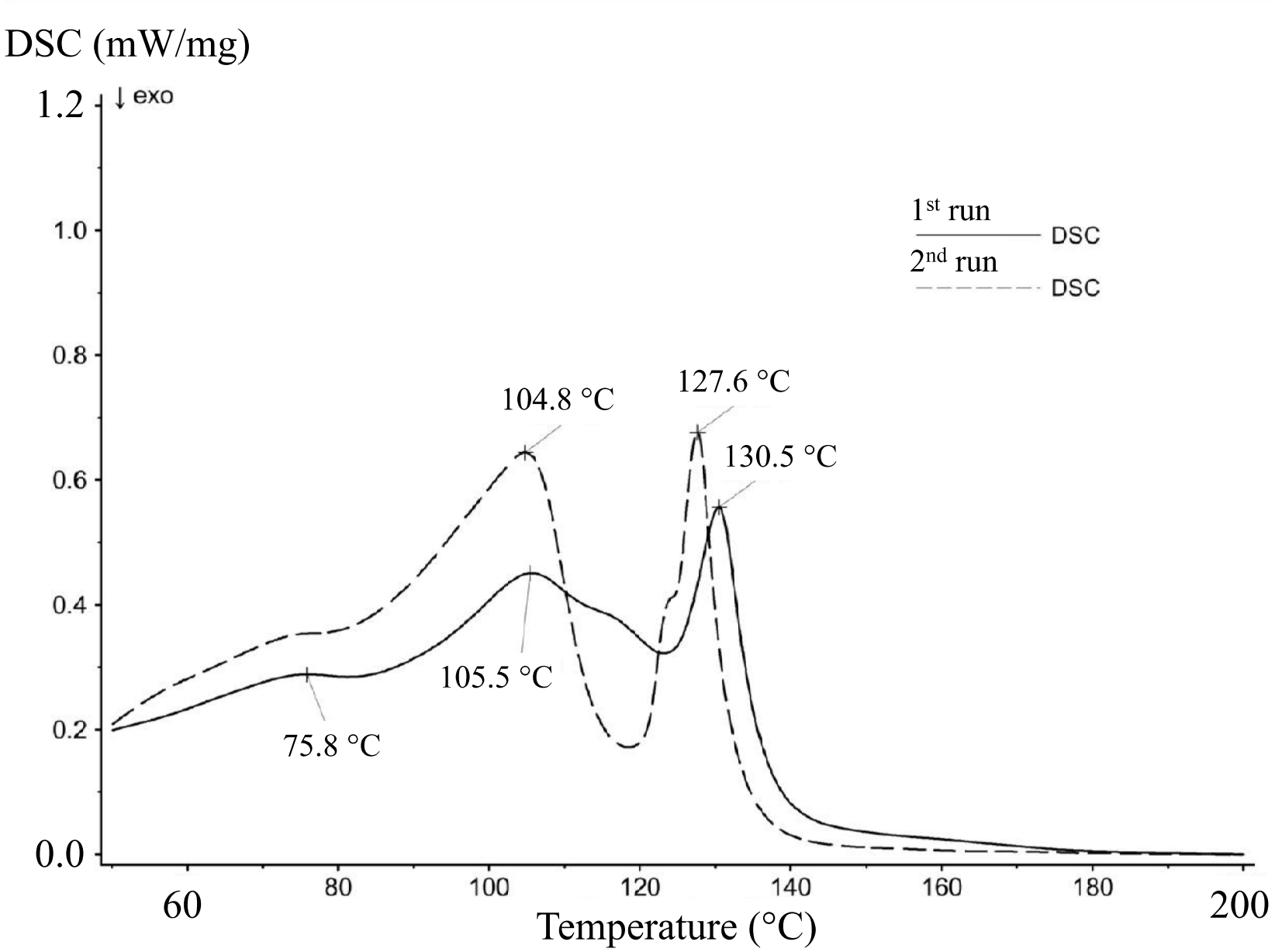

Figure 12-d: DSC results - Part #4 Srf - 1st and 2nd run